



1 **Spatial Disparities of Ozone Pollution in the**
2 **Sichuan Basin Spurred by an Extreme Heatwave**

3

4 Nan WANG^{1*}, Yunsong DU¹, Dongyang CHEN¹, Haiyan MENG¹, Xi

5 CHEN², Li ZHOU¹, Guangming SHI¹, Yu ZHAN¹, Miao FENG³, Wei LI³,

6 Mulan CHEN⁴, Zhenliang LI⁴, Fumo YANG^{1*}

7

8 ¹College of Carbon Neutrality Future Technology, Sichuan University, Chengdu, China

9 ²Institute of Mass Spectrometry and Atmospheric Environment, Guangdong Provincial
10 Engineering Research Center for On-line Source Apportionment System of Air
11 Pollution, Jinan University, Guangzhou, PR China

12 ³Chengdu Academy of Environmental Sciences, Chengdu, 610072, China

13 ⁴Chongqing Research Academy of Eco-Environmental Sciences, Chongqing, 401147,
14 China

15

16 Correspondence to fmyang@scu.edu.cn, nan.wang@scu.edu.cn

17

18 **KEYWORDS:** ozone pollution, heatwave, spatial disparity, Sichuan

19 Basin, ozone formation mechanism

20

21



22

Abstract

23 Under the influence of climate change, the increasing occurrence of extreme weather
24 events, such as heatwaves, has led to an enhanced frequency of ozone (O₃) pollution
25 issues. In August 2022, the Sichuan Basin (SCB), a typical large-scale geographical
26 terrain located in southwestern China, experienced the most severe heatwave over the
27 last 20 years. The heatwave led to substantial disparities in O₃ levels across the region.
28 Here, by integrating observations, machine learnings and numerical simulations, we
29 aim to understand the diverse O₃ formation mechanisms in two mega cities, Chengdu
30 (western location) and Chongqing (eastern location). Observational data showed that
31 Chengdu experienced a consecutive 17-day period of O₃ exceedance, in contrast to
32 Chongqing, where O₃ concentrations remained below the standard. Meteorological and
33 precursor factors were assessed, spotlighting high temperatures, intense solar radiation,
34 and overnight accumulative pollutants as key contributors to O₃ concentrations. The
35 interplay of isoprene, temperature, and O₃, alongside the observation-based box model
36 and MEGAN simulations, underscored the significant role of intensified biogenic
37 VOCs (BVOCs) on O₃ formations. Interestingly, Chongqing exhibited nearly double
38 the BVOCs emissions of Chengdu, yet contributed less to O₃ concentrations. This
39 discrepancy was addressed through CMAQ-DDM simulations and satellite diagnosis
40 by investigating the O₃-NO_x-VOCs sensitivity. Notably, Chengdu displayed a VOCs-
41 driven sensitivity, while Chongqing showed a transitional regime. Moreover, the
42 regional transport also played a pivotal role in the spatial divergence of O₃ pollution.
43 Cross-regional transport predominantly influenced Chongqing (contributing ~80%),
44 whereas Chengdu was mainly affected by the emissions within the basin. The local
45 accumulated pollutants gave rise to the atmospheric oxidizing capacity, resulting in a
46 substantial photochemical contribution to O₃ levels (49.9 ppbv/hour) in Chengdu. This
47 comparison of the difference provides the insights into the complex interplay of
48 meteorology, natural emissions, and anthropogenic sources during heatwaves, guiding
49 the necessity of targeted pollution control measures in regional scales.



50 **1 Introduction**

51 Ground-level ozone (O_3), formed through intricate photochemical
52 reactions involving precursors like volatile organic compounds (VOCs)
53 and nitrogen oxides (NO_x) under sunlight, is a prominent constituent of
54 smog and a major contributor to poor air quality. Different from the
55 protective role in the stratosphere, O_3 in the troposphere has garnered great
56 attention due to its potential damage to human well-being and ecological
57 systems (Krupa and Kickert, 1989; Schwela, 2000; Emberson et al., 2001;
58 Xiao et al., 2021). The hazardous effects span across multiple domains,
59 such as detrimental impact on human health, vegetation growth, and the
60 climate. Addressing O_3 pollution is a complex endeavor, which mainly
61 arises from the nonlinear relationship between O_3 and its precursors.
62 Besides, the substantial influence of meteorological conditions adds
63 another layer of intricacy to the challenge of managing O_3 pollution. Under
64 global warming, the interplay of factors such as extreme weather events
65 and elevated anthropogenic emissions have led to the frequent emergence
66 of O_3 pollution, exacerbating air quality issues in urban areas worldwide.
67 Net O_3 production arises when the equilibrium between O_3 and nitrogen
68 oxides (NO_x), i.e., $NO + O_3 \rightarrow NO_2 + O_2$, is disrupted through the
69 involvement of alkylperoxyl (RO_2) and hydroperoxyl (HO_2) radicals
70 originating from oxidation of VOCs and carbon monoxide (CO). This
71 intervention triggers the oxidation of NO to NO_2 , ultimately resulting in
72 the accumulation of O_3 through NO_2 photolysis (Jacob, 2000; Lelieveld
73 and Dentener, 2000). Functioning as a pivotal role in photochemical
74 reactions, VOCs have been identified as a crucial focal point for advancing
75 efforts in the prevention and management of O_3 pollution (Jenkin and
76 Clemitshaw, 2000). However, influenced by the diversity, abundance and
77 reactivity of VOCs species, the spatial and temporal of VOCs
78 characteristics depict regional disparities, adding difficulty in developing
79 an effective strategy to reduce photochemical smog. Moreover, due to the
80 dual roles of NO_x in O_3 formation, where they enhance O_3 formation in low
81 NO_x environments and titrate O_3 in high NO_x environments, reductions in
82 VOCs must be examined along with the patterns of NO_x . Given the diverse
83 energy structures in different regions, comprehending the regional



84 responsiveness of O₃-NO_x-VOCs sensitivity is essential. This is
85 particularly vital for elucidating non-linear relationship discrepancies
86 within regional contexts, which helps to advance the formulation of
87 effective emission reduction strategies.

88 O₃ pollution episodes are also closely related to meteorology. High
89 temperature, intensive solar radiation and light winds are found to be the
90 unfavorable weather conditions inducing photochemical pollutions (Ding
91 et al., 2017; Wang et al., 2017; Wang et al., 2022b). Generally, the impact
92 of meteorological conditions on O₃ is manifested through factors such as
93 changes in chemical reaction rates, dry/wet deposition, and atmospheric
94 transport. By objectively classifying pollution weather types, numerous
95 studies have summarized the typical weather conditions that lead to O₃
96 pollution. For example, high-pressure ridge, continental anticyclone and
97 the periphery of typhoons are the typical weather system conducting O₃
98 pollutions in east Asia (Mcelroy et al., 1986; Daum et al., 2003; Wang et
99 al., 2015). Besides, meteorology can also indirectly affect O₃ by
100 modulating natural emissions, such as BVOCs (biogenic VOCs) emissions
101 from vegetation and reactive nitrogen emissions from soil (Hall et al., 1996;
102 Saunier et al., 2017; Huang et al., 2018). For instance, a rise in temperature
103 can result in elevated emissions of BVOCs, thereby contributing to the
104 formation of O₃ (Wang et al., 2022b). With the influence of climate change,
105 there is an increasing frequency of extreme weather events, further
106 perturbing the natural emissions and finally exacerbating O₃ pollutions
107 (Lu et al., 2019).

108 The Sichuan Basin (SCB), encircled by the Qinghai-Tibet Plateau, Yungui
109 Plateau, and surrounding mountain ranges, stands as a notable hotspot for
110 atmospheric pollution within China. Two mega cities, Chengdu and
111 Chongqing, are situated in the SCB with populations exceeding 50 million.
112 In fact, a considerable amount of research on the pollution characteristics
113 of O₃ has been conducted in the SCB. For example, the characteristics of
114 O₃ and the precursors have been widely measured and analyzed (Zhao et
115 al., 2018; Qiao et al., 2019; Zhou et al., 2020; Chen et al., 2022). The
116 complicated coupling effect between the plateau-deep basin topography
117 and the unique meteorological conditions on atmospheric pollution have



118 been studied (Hu et al., 2022; Shu et al., 2022; Lei et al., 2023). The impact
119 of aerosol feedbacks on O₃ was also explored (Wang et al., 2020).

120 However, a limited focus has been placed on contrasting the varied
121 responses among different sites or cities within the basin. Exploring and
122 contrasting diverse mechanisms across multiple sites enriches our
123 comprehension and facilitates collaborative air pollution mitigation efforts
124 in a regional scale. In August 2022, the SCB experienced an exceptionally
125 rare heatwave, with monthly mean temperature ranking the highest over
126 the last two decades. As a result, the Chengdu Plain suffered from 17-day
127 consecutive O₃ pollution, whereas Chongqing remained good air quality.
128 Here, we combined field measurements, machine learning and numerical
129 simulations to elucidate the spatial disparities of O₃ pollution mechanism
130 within the SCB. This information has implication for better understanding
131 the meteorological contributions, discrepancy in O₃-NO_x-VOCs sensitivity,
132 and regional transport disparities between large urban areas, and provides
133 insights for regional joint control of O₃ pollution.

134 **2 Method**

135 **2.1 Data Source**

136 Data of atmospheric compositions, including O₃, NO_x (NO and NO₂), CO,
137 SO₂, VOCs components and meteorological parameters were collected
138 from two in-situ observational sites. One was the Junping Street Station in
139 Chengdu and the other was the Academy of Environmental Sciences
140 Station in Chongqing. Both sites situated in the urban center of Chengdu
141 and Chongqing, representing the air quality of urban sites. Detailed
142 information of the measurements, such as monitoring instruments, data
143 coverage, and resolution were summarized in Table S1. Briefly, the
144 ambient concentrations of O₃, NO_x, CO and SO₂ were detected by
145 instruments produced by Thermo Scientific (Model 49i, 42i, 48i and 43i,
146 respectively). The species of VOCs were sampled by the GC955-611/811
147 Ozone Precursor Analyser produced by Synspec. Meteorological
148 parameters including temperature, relative humidity, wind speed and wind
149 direction at the same sites were concurrently measured by the mini-weather
150 stations (WS600-UMB in Chengdu and WS502-WTB100 in Chongqing).



151 All instruments were meticulously maintained and regularly calibrated.
152 Moreover, the air quality monitoring network established by the Ministry
153 of Ecology and Environment of China was employed to assess O₃ pollution
154 events in the SCB.

155 2.2 Stepwise Regression Analysis

156 We employed the stepwise regression analysis to assess the impact of
157 various meteorological factors on O₃ formation. This approach involves the
158 introduction of numerous input variables, with the method iteratively
159 selecting significant factors while eliminating non-significant ones,
160 ultimately resulting in the identification of a final set of critical factors.
161 Following this, we constructed a multivariate linear regression equation to
162 model O₃ concentration. In detail, meteorological parameters were
163 obtained from the fifth generation of the European Centre for Medium-
164 Range Weather Forecasts atmospheric reanalysis (ERA5). The selected
165 parameters included 10m u-component of wind (U10), 10m v-component
166 of wind (V10), vertical wind (w), boundary layer height (BLH), 2m
167 temperature (T2) and surface solar radiation (SSR). Given the high
168 correlation (R=0.85) between the diurnal variations of T2 and SSR during
169 the heatwave, it was challenging to distinguish the individual impacts of
170 T2 and SSR. As a pragmatic approach, we chose to combine them by
171 multiplying T2 with SSR, thereby examining the collective influence of
172 elevated temperatures and high solar radiation. Additionally, we also
173 incorporated previous night accumulative air pollutants, such as O₃
174 (ACCO₃) and NO₂ (ACCNO₂), as input parameters to investigate the
175 impact of pollutants being overnight accumulated on O₃ levels. The
176 machine learning-simulated O₃ concentrations were then validated against
177 observations, revealing a robust correlation (R > 0.91, P < 0.01) between
178 them (Fig S1). This result demonstrates the effectiveness of meteorological
179 and overnight accumulative factors in explaining a substantial portion of
180 O₃ concentrations.

181 2.3 Observation-based model (OBM)

182 In this study, an observation-based box model (OBM) configured with the
183 master chemical mechanisms (MCM v3.3.1) was employed to identify the



184 key VOCs species influencing O₃ (Jenkin et al., 2015; Bloss et al., 2005;
185 Saunders et al., 2003; Jenkin et al., 2003; Jenkin et al., 1997). The model
186 considered VOCs concentrations, trace gases (O₃, NO_x, CO, SO₂),
187 meteorological parameters, as well as the photolysis rates of NO₂ (J_{NO₂})
188 from the in-situ sites in Chengdu and Chongqing. Observations were used
189 as constraints in the model and were averaged to represent the diurnal cycle
190 with a time resolution of 1 hour. The photolysis rates generated by the
191 model were adjusted based on the measured J_{NO₂} values in order to
192 accurately simulate the photochemical reactions. The mean mixing ratios
193 of 46 VOCs species, including 20 alkanes, 11 alkenes, 1 alkyne (ethyne)
194 and 14 aromatics were listed in Table S2. The model started at 00:00 local
195 time (LT) and ran for a period of 24 hours. Prior to the formal calculation,
196 we conducted a spin-up run for 4 days with constraints representing the
197 diurnal cycle, allowing the unconstrained compounds (e.g., radicals and
198 HCHO) to reach steady states. Using the OBM simulation, the relative
199 incremental reactivity (RIR) method was applied to assess the sensitivity
200 of O₃ formation to individual precursor species (Cardelino and Chameides,
201 1995; Meng et al., 2023; Zhang et al., 2019; Xue et al., 2014; Zhu et al.,
202 2020). The calculation process can be expressed in Eq. (1).

$$203 \quad \text{RIR}(X) = \frac{(P_{\text{O}_3}(X) - P_{\text{O}_3}(\Delta X)) / P_{\text{O}_3}(X)}{\Delta C(X) / C(X)} \quad (1)$$

204 Here, X represents a specific precursor of O₃. $P_{\text{O}_3}(X)$ and $P_{\text{O}_3}(\Delta X)$
205 represent the maximum simulated O₃ concentration based on measured
206 concentration and the concentration when the precursor levels change by
207 ΔX . $\Delta C(X) / C(X)$ indicates the relative change of precursor X . In this study,
208 a reduction of 20% in precursor X was selected to perform the RIR analysis.

209 **2.4 Lagrangian Particulate Dispersion Modeling**

210 We conducted backward Lagrangian particulate dispersion modeling
211 (LPDM) to ascertain the potential source regions for the air masses
212 observed at the monitoring stations. This approach involved employing the
213 hybrid single-particulate Lagrangian-integrated trajectory model
214 (HYSPLIT) driven by the ARL format Global Data Assimilation System
215 (GDAS) data. The LPDM was executed with a temporal resolution of 1



216 hour, releasing 3000 particulates at 100 meters above sea level from the
217 site and then tracking their backward movement for 72 hours. The
218 particulates' positions were calculated in both vertical and horizontal
219 dimensions, considering the impact of atmospheric advection and diffusion.
220 By analyzing the resulting data, we derived the "retroplume", which
221 indicates the spatial residence time of particulates and reflects the
222 distribution of surface probability or simulated air mass residence time.
223 This technique enabled us to diagnose whether the in-situ observation was
224 predominantly influenced by local emissions or regional transport.

225 **2.5 Chemical transport modeling**

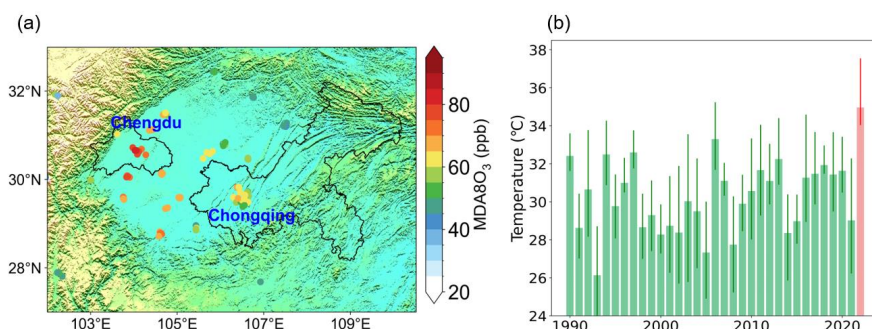
226 A chemical transport model, WRF-MEGAN-CMAQ (Weather Research
227 Forecast – Model of Emissions of Gases and Aerosols from Nature –
228 Community Multiscale Air Quality), was employed to study the O₃
229 formation mechanism in the SCB. We adopted a two-nested domain, with
230 the outer domain covering most parts of east Asia (grid resolution of 36×
231 36 km) and the inner domain covering the southwestern China with the
232 SCB being focused (grid resolution of 12×12 km). The European Center
233 for Medium-Range Weather Forecasts (ECMWF) reanalysis data was used
234 as the initial and lateral boundary conditions of the WRF (version 3.9.1).
235 Carbon Bond Mechanism Version 6 and Aerosol Scheme 6 were used for
236 gas-phase and aerosol chemical simulations within the CMAQ model
237 (version 5.4), respectively. With regard to anthropogenic emissions, the
238 recently updated 2020-based MEIC emissions (Multi-resolution Emission
239 Inventory for China, developed by Tsinghua University) were used for
240 areas within China and the 2010-based MIX emissions (Li et al 2017) were
241 used for regions outside China. Both sets of the emissions have a horizontal
242 resolution of 0.25×0.25°, incorporating sectors such as transportation,
243 industry, power plant, residential and agriculture. Besides, natural
244 emissions were calculated using MEGAN model (version 2.1) driven by
245 the WRF simulated meteorology. The static input vegetation-related data
246 of MEGAN were updated by using the 2020-based the plant function type
247 (PFT) and leaf area index (LAI) retrieved from the MODIS (Moderate-
248 Resolution Imaging Spectroradiometer) products. More details of the



249 modeling configuration were summarized in Table S3.
250 In this study, we introduced the CMAQ-DDM (Decoupled Direct Method)
251 module to investigate the non-linear relationship between O₃ and its
252 precursors. Unlike the traditional brute force method (BFM) that involves
253 cutting or eliminating emissions from source regions (or sectors), which is
254 not only computationally intensive but also prone to uncertainties (due to
255 the intricate non-linear nature of O₃ chemistry), the DDM method offers a
256 more refined alternative. It enables accurate and computationally efficient
257 calculations of the sensitivity coefficients required for evaluating the
258 impact of parameter variations on output chemical concentrations
259 (Napelenok et al., 2008). Herein, both first-order and higher order
260 sensitivities were calculated to obtain the O₃-NO_x-VOCs sensitivities in
261 Chengdu and Chongqing. Furthermore, we also utilized the CMAQ-ISAM
262 (Integrated Source Apportion Method) technique, an innovative approach
263 for source tracing. This method enables us to trace and quantify the distinct
264 impacts on O₃ concentrations originating from specific source sectors,
265 emissions confined within designated geographical regions, as well as
266 effects arising from stratospheric and lateral boundary conditions (Kwok
267 et al., 2013). Through this approach, we calculated the separate influences
268 of anthropogenic and biogenic emissions on O₃ levels. We also assessed
269 the contributions of source regions to O₃ levels in Chengdu and Chongqing,
270 encompassing both local and regional influences. A map of source region's
271 classification in this study was provided in Fig S2.
272 We validated the performance of the WRF-MEGAN-CMAQ model using
273 surface network monitoring data. The time series and statistical outcomes
274 of the simulated and observed O₃ within the SCB are consolidated in Fig
275 S3. In general, the favorable alignment between observations and
276 simulations underscores the model's proficiency in accurately replicating
277 the magnitude and temporal variations of air pollutants.

278 **3 Results and discussion**

279 **3.1 Regional disparity of O₃ between Chengdu and Chongqing**



280

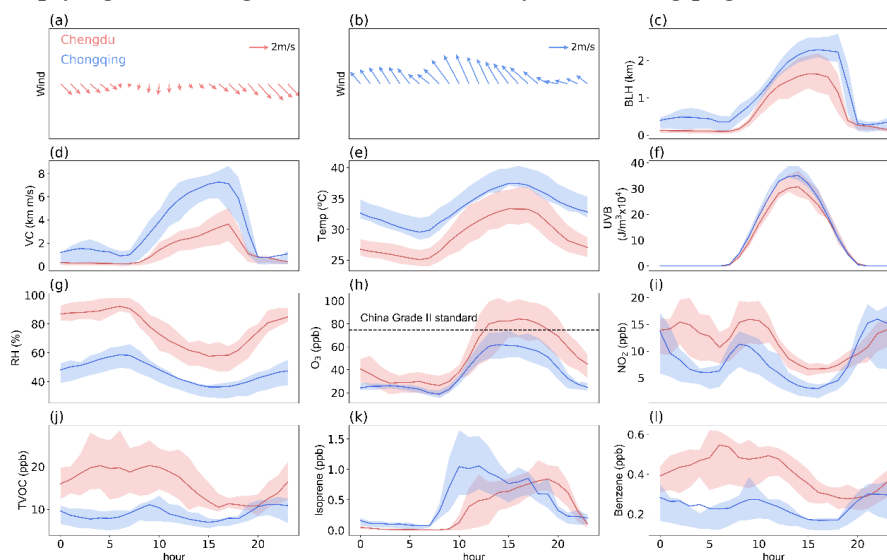
281 Fig 1 (a) Geographical distribution of Sichuan Basin with scattered averaged monthly MDA8
282 O₃ concentrations (data obtained from Ministry of Ecology and Environment of China). The
283 black lines highlight the administrative border of Chengdu and Chongqing, respectively. (b)
284 Historical monthly averaged daily-maximum air temperature (August) variation of the SCB
285 from 1990 to 2022. The red bar highlights the extreme hot temperature in 2022.

286 August 2022 witnessed the SCB experiencing its hottest August in the last
287 20 years, with Chengdu and Chongqing reporting monthly mean
288 temperatures soaring to 36.8°C and 40.3°C, respectively (Fig 1). Typically,
289 the atmospheric conditions in the SCB are relatively stable due to the
290 topography of the basin. This stability, in conjunction with elevated
291 temperatures, tended to foster the occurrence of photochemical pollution
292 (Zhao et al., 2018; Chen et al., 2022). However, during this historically
293 unprecedented heatwave, O₃ levels exhibited substantial variations across
294 the SCB. Observations revealed that O₃ concentrations surpassed China's
295 Grade II standard (75 ppbv) in the western part of the SCB, notably in
296 Chengdu. Conversely, significantly lower concentrations, well below the
297 standard, were observed in the eastern region of the basin, particularly in
298 Chongqing (Fig 1a). According to the network monitoring data, the average
299 maximum daily 8-hour (MDA8h) O₃ concentration in Chengdu was
300 measured at 75.1 ppbv. In contrast, the MDA8h O₃ concentration in
301 Chongqing was recorded at 55.1 ppbv.

302 Based on the synoptic weather system, it could be found that the SCB was
303 influenced by two dominant weather systems, the South Asia High and the
304 Western Pacific Subtropical High (Fig S4). The former was positioned at
305 the upper troposphere (around 200 hpa), with its center located in the
306 northern part of the SCB. Meanwhile, the latter was situated within the



307 troposphere (lower than the former), with its high-pressure ridge extending
308 from east to west, covering the entire SCB region. Under the influence of
309 the two major high-pressure systems, the SCB experienced subsidence
310 airflows, resulting in a stationary atmospheric structure. According to the
311 synoptic flows (Fig S4), it could be seen the prevailing wind was
312 southeastward, and the wind speed gradually decreased from east to west,
313 implying that Chengdu was more stationary than Chongqing.



314
315 Fig 2 Diurnal variation of meteorological parameters (including winds, boundary layer
316 height (BLH), temperature (temp), relative humidity (RH) and ultraviolet radiation (UVB))
317 and air pollutants (O₃, NO₂, total volatile organic carbons (TVOC) and isoprene) in Chengdu
318 and Chongqing, respectively

319 Furthermore, we compared the averaged diurnal variations of the in-situ
320 measured meteorological parameters and air pollutants (Fig 2). Consistent
321 with the analysis of weather patterns, Chongqing was influenced by the
322 southeast winds (3.1 m/s), while Chengdu was more stagnant with lighter
323 wind speed (1.4 m/s) (Fig 2a-b). In addition, the boundary layer height
324 (BLH) was also significantly higher in Chongqing (Fig 2c). A simple
325 calculation of the ventilation coefficient (VC) with wind speed and BLH
326 indicated that Chongqing (VC=3.34 km·m/s) had better ventilation
327 conditions compared to Chengdu (VC=1.24 km·m/s, Fig 2d). It could be
328 inferred that, influenced by lighter winds and lower BLH, air pollutants in
329 Chengdu were more easily trapped and accumulated. Both cities displayed

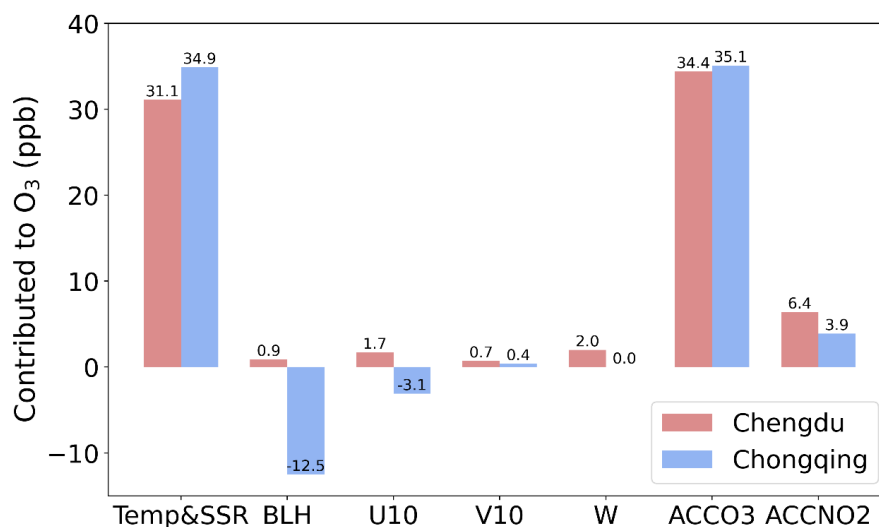


330 typical meteorological features of a heatwave conducive to photochemical
331 pollution, characterized by elevated temperatures, intense solar radiation,
332 and low relative humidity (Fig 2e-2g). Among these factors, both
333 temperature and solar radiation in Chongqing were higher compared to
334 those in Chengdu, suggesting that the conditions in Chongqing were more
335 conducive to photochemical O₃ reactions. However, the degree of O₃
336 pollution was quite the opposite as previously mentioned (Fig 1a and Fig
337 2h). We conducted further investigation into the diurnal variation of the
338 precursors. Two distinct peaks in NO₂ levels were identifiable, with one
339 occurring in the morning and the other appearing during night (Fig 2i). The
340 morning peaks were likely influenced by vehicular emissions during rush
341 hours. The night peaks were possibly caused by the NO_x titration effect.
342 Moreover, the levels of total VOCs (TVOC) were much higher in Chengdu
343 than those in Chongqing (Fig 2j). Considering the different degrees of NO₂
344 and TVOC concentrations in Chengdu and Chongqing, it could be inferred
345 that there might be differences in the O₃ formation mechanism between the
346 two cities. Indeed, the diurnal variation of isoprene, a highly active VOCs
347 compound, showed distinct differences (Fig 2k). The observed data in
348 Chongqing showed a notable afternoon peak, whereas in Chengdu, the
349 peak appeared exclusively between 17:00 and 20:00. Usually, isoprene,
350 mainly emitted by vegetation, is sensitive to ambient temperature and solar
351 radiation and peaks at noon time. There might be some potential
352 explanations. Firstly, the isoprene peak between 17:00 and 20:00 in
353 Chengdu could be attributed to other sources, such as vehicular emissions.
354 However, this possibility was ruled out after examining the diurnal
355 variation of benzene (Fig 2l). As a marker of anthropogenic vehicular
356 emissions, benzene did not exhibit any peaks between 17:00 and 20:00.
357 The second possibility was that the atmospheric oxidizing capacity in
358 Chengdu was more robust than in Chongqing, leading to the rapid
359 photochemical consumption of isoprene emitted by vegetation. This
360 hypothesis was supported by the diurnal variations in O₃ levels, which were
361 notably elevated in the afternoon, implying of a stronger atmospheric
362 oxidizing capacity. The instrument-detected of isoprene was indicative of
363 its "aged" state, implying the rapid photochemical consumption due to both



364 the atmospheric oxidizing capacity and the inherent reactivity of isoprene
365 itself. Furthermore, a distinct decrease of BLH between 17:00 and 20:00
366 was also a possible reason causing the isoprene peak of Chengdu in the late
367 afternoon.

368 Subsequently, we employed a machine learning method, the Stepwise
369 Regression Analysis, to quantify the impact of diverse meteorological
370 parameters and precursor concentrations on O₃ levels. In both cities, the
371 significance of T2 and SSR, along with ACCO₃ and ACCNO₂, took
372 precedence. This indicates that meteorological conditions characterized by
373 high temperatures, intense solar radiation, and the presence of overnight
374 accumulative pollutants played a pivotal role in O₃ concentration,
375 especially during heatwaves. The distinction between the two cities lied in
376 the significance of atmospheric dispersion capacities represented by the
377 variations in winds and BLH. The study revealed that winds, including both
378 horizontal winds (U10 and V10) and vertical wind (W), along with BLH,
379 had positive effects in elevating O₃ levels in Chengdu. Conversely, they
380 predominantly had negative effects, resulting in a decrease in O₃ levels, in
381 Chongqing. These findings align with the diurnal analysis, which indicated
382 that Chengdu experienced lighter winds and lower BLH. The poor
383 ventilation conditions facilitated the accumulation of air pollutants,
384 contributing to the increase in O₃ levels. In contrast, the ventilation
385 condition in Chongqing was conducive to reduce O₃ concentrations.
386 Combined with the aforementioned analysis of diurnal patterns, it could be
387 inferred that Chengdu was more constrained by local emissions, while
388 Chongqing was more susceptible to regional transport influences (further
389 discussed in Section 3.3).



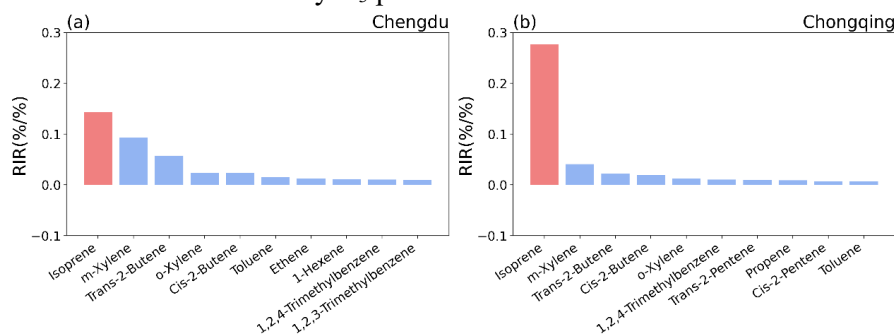
390
391 Fig 3 Contribution of multi-factors influencing O₃ concentrations in Chengdu and Chongqing,
392 respectively

393 3.2 Difference in heatwave-intensified BVOCs emissions and 394 their impact on O₃ formation

395 In addition to the influence of meteorological factors under heatwave
396 conditions, the precursors also play important roles in contributing O₃
397 concentrations. Therefore, we utilized the OBM model to compute and
398 identify the primary VOCs components that exerted a substantial influence
399 on O₃ levels. Here, we introduced the RIR values that could reflect the
400 importance of a given species to O₃ concentrations. As Fig 4 shows,
401 Alkenes and aromatic hydrocarbons were the principal VOCs components
402 influencing O₃ levels in both cities. In Chengdu, the most influential VOCs
403 species on O₃ concentrations included isoprene, m-xylene, trans-2-butene,
404 o-xylene, cis-2-butene, toluene, ethene, 1-hexene, 1,2,4-trimethylbenzene,
405 and 1,2,3-trimethylbenzene. Similarly, in Chongqing, the primary VOCs
406 contributors to O₃ levels were isoprene, m-xylene, trans-2-butene, cis-2-
407 butene, o-xylene, 1,2,4-trimethylbenzene, trans-2-pentene, propane, cis-2-
408 pentene, and toluene. According to the results, both Chengdu and
409 Chongqing should prioritize the regulation of alkenes and aromatic
410 hydrocarbons from sources like vehicular emissions and solvent usage.
411 Besides, the results clearly highlight isoprene as the dominant VOCs
412 species impacting O₃ levels. The characteristics of the heatwave were high

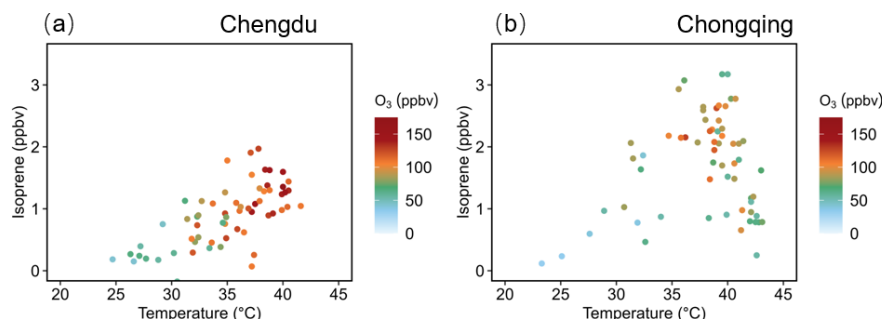


413 temperature, intense solar radiation and dry air condition. These
 414 meteorological factors significantly enhanced the emission of BVOCs
 415 from vegetation, indicating the notable role of heatwave-triggered natural
 416 emissions in the secondary O₃ pollution.



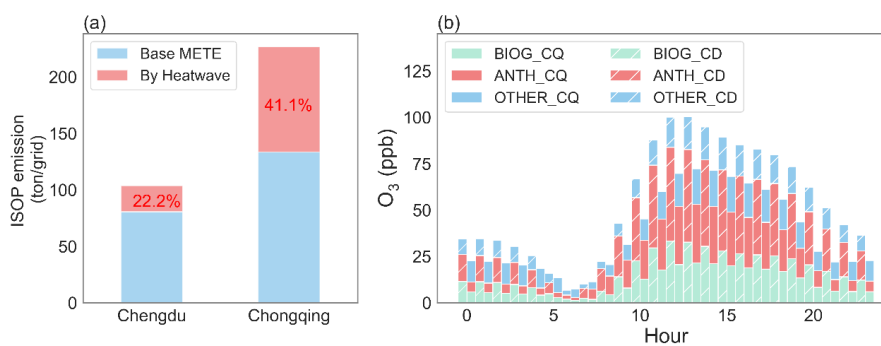
417
 418 Fig 4 OBM calculated the top 10 VOCs species with the highest RIR values in (a) Chengdu
 419 and (b) Chongqing.

420 We further examined the relationship between isoprene, temperature, and
 421 O₃ using observational data. In order to expand the sample size, we
 422 gathered a dataset corresponding to the daily maxima O₃ values recorded
 423 during the months of July and August in 2022. In Chengdu, the variations
 424 of isoprene and temperature basically showed an increasing trend,
 425 indicating that higher isoprene concentrations were associated with higher
 426 temperatures, which in turn coincided with elevated O₃ levels (Fig 5a). In
 427 Chongqing, the concentration of isoprene initially increased with rising
 428 temperatures. However, when the temperature surpassed approximately
 429 40°C, the isoprene concentration started to decrease with further
 430 temperature elevation (Fig 5b). Notably, the peak values of O₃
 431 corresponded closely to the high values of isoprene, occurring at
 432 temperatures ~ 38°C to ~ 42°C. According to recent studies, isoprene
 433 emissions increase with rising temperatures, and even under high-
 434 temperature conditions when vegetation closes stomata, due to the indirect
 435 impact of elevated leaf temperature, it decreases only under extreme high-
 436 temperature drought conditions because of the inhibition of substrate
 437 supply (Potosnak et al., 2014; Wang et al., 2022a). Here, the variation of
 438 isoprene with temperature in Chengdu and Chongqing illustrates these two
 439 distinctions though the isoprene concentration being observed was “aged”.



440
441 Fig 5 Scatter plots of observed isoprene, temperature and O₃ in (a) Chengdu and (b)
442 Chongqing. The data were collected corresponded to daily maxima O₃ concentrations from
443 July 2022 to August 2022.

444 We utilized the theoretical calculation from MEGAN model to quantify the
445 disparities in isoprene emissions between the two cities. Considering the
446 varying administrative areas of Chengdu (14,378 km²) and Chongqing
447 (82,339 km²), comparing the total isoprene emissions might not be
448 appropriate. Instead, we quantified the emissions per unit grid area (9×9
449 km) for both locations (Fig 6). It can be observed that the isoprene
450 emissions in Chongqing were higher than those in Chengdu (nearly twice
451 as much). In particular, under the influence of heatwaves, the isoprene
452 emissions in Chongqing and Chengdu increased by 41.1% and 22.2%,
453 respectively. The significant role of heatwave-intensified BVOCs
454 emissions was expected to aggravate O₃ pollution in Chengdu and
455 Chongqing. With the aid of CMAQ-ISAM simulation, we proceeded to
456 quantify the distinct impacts of anthropogenic emissions and BVOCs
457 emissions on O₃ concentrations. The findings indicated that at 13:00 (local
458 time), when photochemical reactions were most intense, anthropogenic
459 emissions contributed to 50.6 ppbv and BVOCs emissions contributed to
460 33.3 ppbv in Chengdu. In comparison, anthropogenic emissions and
461 BVOCs emissions contributed to 31.3 ppbv and 20.6 ppbv in Chongqing,
462 respectively. Interestingly, despite higher BVOCs emissions in Chongqing
463 compared to Chengdu, the contribution of BVOCs to O₃ levels was actually
464 smaller in Chongqing than in Chengdu. This implies that there were
465 differences in the O₃-NO_x-VOCs response mechanisms between the two
466 cities.



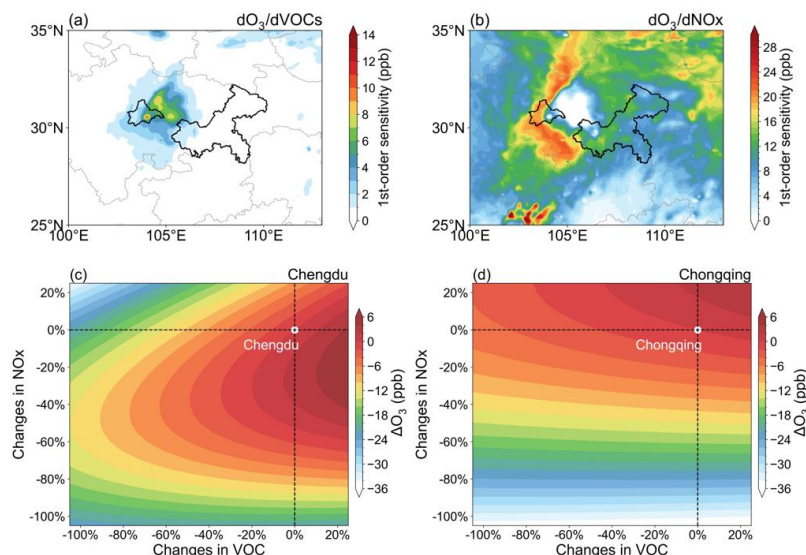
467

468 Fig 6 (a) Meteorology driven ISOP emission between Chengdu and Chongqing, respectively;
469 (b) Averaged source contributions (by emissions) to diurnal O₃ levels in Chengdu (CD) and
470 Chongqing (CQ), respectively. BIOG, ANTH and OTHER refer to contributions from the
471 biogenic, the anthropogenic and the others.

472 Herein, we conducted CMAQ-DDM simulations to investigate the
473 nonlinear relationship between O₃ and its precursors. Indeed, the O₃-NO_x-
474 VOCs sensitivity response mechanisms in Chengdu and Chongqing were
475 of difference (Fig 7 a-b). On the one hand, the Chengdu region
476 demonstrated a greater sensitivity (first-order sensitivity coefficients) to
477 VOCs in comparison to Chongqing. Specifically, in certain urban grids
478 within Chengdu, the sensitivity coefficient exceeded 10 ppbv, while the
479 highest sensitivity in Chongqing was only ~ 3 ppbv. On the other hand,
480 Chongqing generally exhibited higher sensitivity to NO_x, except for quite
481 limited urban cores. In contrast, the eastern areas of Chengdu, particularly
482 its urban cores, displayed low sensitivity to NO_x. Furthermore, by taking
483 both the first-order sensitivity coefficient and the 2nd-order sensitivity
484 coefficient into account, we constructed the O₃ isopleth for both cities
485 during the month of August (Fig 7 c-d). It was evident that Chengdu was
486 situated in a VOCs-limited regime, while Chongqing was operating within
487 a mixed-limited regime. These simulated results agree with the satellite
488 diagnosed O₃ formation sensitivity (obtained through the ratio of HCHO
489 and NO₂), confirming again the good modeling performance (Fig S5). The
490 results implied that a temporary decrease in NO_x emissions in Chengdu
491 would result in an increase in O₃ concentrations, whereas reducing VOCs
492 emissions could potentially lower O₃ pollution. This finding could partially
493 explain the increasing trend of O₃ concentrations in Chengdu Plain during



494 the past as the previous emission control measures were mainly targeted to
 495 NO_x emissions (driven by the need to control acid rain and PM_{2.5} pollution,
 496 successively). In Chongqing, differently, a reduction in either NO_x
 497 emissions or VOCs emissions could contribute to alleviating O₃ pollution.
 498 The disparity in O₃-NO_x-VOCs sensitivity between the two cities could
 499 also elucidate the reason why Chongqing, despite its higher BVOCs
 500 emissions, exhibits a lower contribution to O₃ levels. Considering the
 501 varying regional sensitivities in O₃-NO_x-VOCs formation, it is advisable to
 502 implement precise emission reduction strategies tailored to the unique
 503 sensitivities of each city for effective pollution prevention and control. This
 504 approach stands in contrast to a uniform solution that may not suit all
 505 contexts. For example, in Chengdu, the previously nationally implemented
 506 strategy, which prioritized NO_x-focused control, might ultimately lead to
 507 O₃ reduction through substantial NO_x reductions. However, this approach
 508 would initially enter into a phase characterized by relatively high O₃
 509 concentrations (positioned within the transitional regime based on the O₃
 510 isopleth), posing environmental risks. Instead, a strategy centered on VOCs
 511 control alongside simultaneous NO_x control could bypass the "high-O₃"
 512 phase and align with the need to address both O₃ and PM_{2.5} pollution.



513

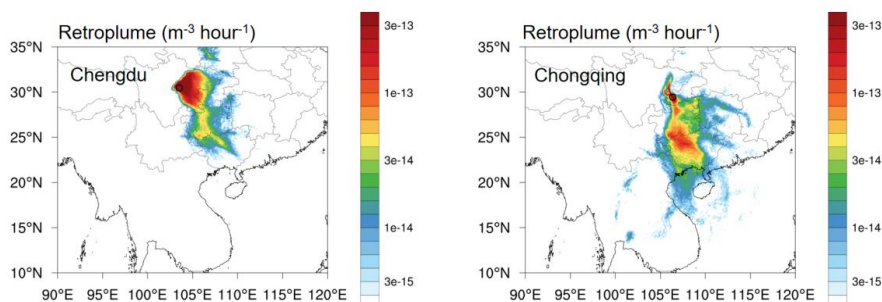
514 Fig 7 Spatial distribution of daytime first-order sensitivity coefficients to (a) VOCs and (b)

515 NO_x; O₃ isopleth plots in (c) Chengdu and (d) Chongqing



516 3.3 Regional divergence of source region contribution

517 Surface-level O₃ is influenced not only by photochemical reactions but also
518 by regional transport. In this section, we mainly focus on the disparities in
519 the impact of regional transport on O₃ between Chengdu and Chongqing.
520 Fig 8 demonstrates the LPDM simulated 72h backward retroplumes
521 influencing Chengdu and Chongqing. In general, Chengdu was primarily
522 influenced by local air masses, encompassing areas such as Chengdu city
523 and the eastern parts of the SCB. Relatively fewer air masses originated
524 from cross-province transport in the southeast direction. Differently,
525 Chongqing showed a situation to be more susceptible to cross-regional
526 transport influences. The dominant air masses in Chongqing not only
527 originated locally but also experienced cross-province transport from the
528 southeast, influenced by the regions such as Guizhou and Guangxi with
529 cleaner ambient air masses. The results from the LPDM simulations closely
530 aligned with the Stepwise Regression Analysis as showed in Section 3.1.
531 Besides, we also adopted the in-situ measured data by comparing the ratio
532 of m, p-xylene and ethylbenzene. Given that m, p-xylene is more reactive
533 than ethylbenzene, their ratios typically decrease due to photochemical
534 reactions that take place during the transport of air masses. As shown in
535 Fig S6, the ratio was much lower in Chongqing (1.04 ppbv ppbv⁻¹),
536 indicating the presence of "aged" air masses being monitored. Conversely,
537 a higher ratio (3.11 ppbv ppbv⁻¹) in Chengdu indicated the prevalence of
538 "fresh" air masses likely originating from local emissions. The discovery
539 reaffirmed that Chongqing exhibited superior ventilation conditions
540 compared to Chengdu. This inference suggests that Chongqing's enhanced
541 dispersion capacity played a pivotal role in significantly reducing its O₃
542 concentrations during the severe heatwave period.



543

544

545

Fig 8 Comparison of 72h retroplume (footprint residence time) showing transport pathways of air masses arriving at Chengdu and Chongqing in August 2022

546

547

548

549

550

551

552

553

554

555

556

557

558

559

560

561

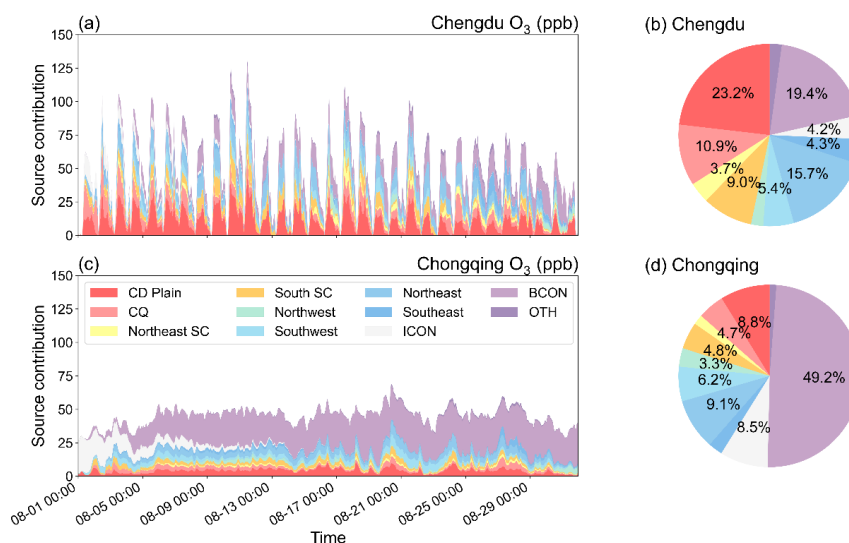
562

563

564

565

Further, we employed the CMAQ-ISMA modeling system to quantify the source region's contribution to Chengdu and Chongqing (Fig 9). In this study, we divided the study area into eight major regions, namely Chengdu Plain (CD Plain), Chongqing (CQ), South Sichuan (South SC), Northeast Sichuan (Northeast SC), Northwest Region (Northwest), Southwest Region (Southwest), Northeast Region (Northeast), and Southeast Region (Southeast) (Fig S2). Generally, the regions like CD Plain, CQ, Northeast SC, South SC were distributed within the SCB region, and could be regarded as the local regions. On the other hand, regions like Northwest, Southwest, Northeast, and Southeast were situated outside the SCB and air masses originating from these regions were considered to be a result of regional transport. As Fig 9 shows, Chengdu was mainly affected by local regions, contributed to 46.8%. This implied that local emissions within the SCB were a significant contributor to the excessive O₃ levels in Chengdu. In contrast, the influence of the local region on O₃ levels in Chongqing was only 18.3%. Instead, the contribution outside the basin almost reached 50%, indicating that Chongqing was more susceptible to the influence of cross-regional transport. This difference demonstrates that even the two major core cities located within the SCB exhibit distinct source contribution characteristics.



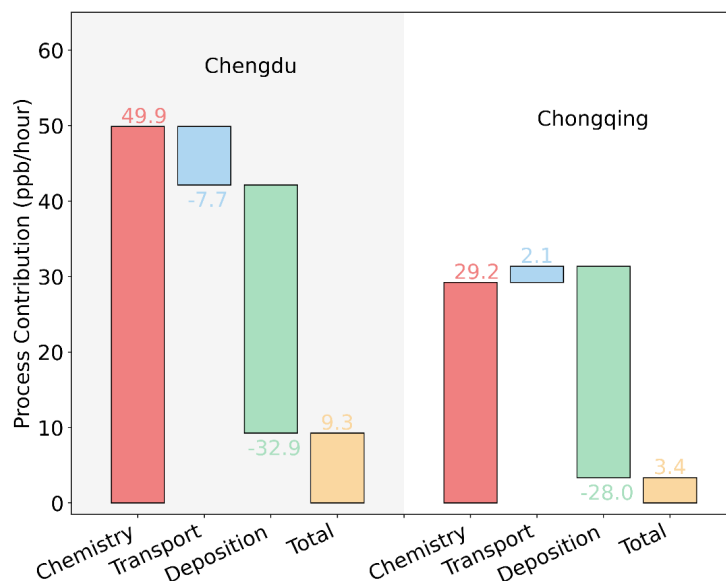
566

567 Fig 9 Source region's contribution to O₃ levels in Chengdu (a) Time series of O₃ contributions
568 from each region. (b) Pie charts illustrating the percentage contributions of each region. (c)
569 and (d) same as (a) and (b), but in Chongqing

570 Given that ambient O₃ concentrations are the integrated results of multiple
571 processes, encompassing photochemical formation, deposition, and
572 transport, we employed the Integrated Process Rate (IPR) tool within the
573 CMAQ model to analyze the contributions of individual physical and
574 chemical processes to O₃ levels. Here, we compared the contributions of
575 different processes to O₃ during the peak period of heightened
576 photochemical reactions at 14:00 in the afternoon. As Fig. 10 shows, the
577 process analysis results reveal distinct differences between the two cities.
578 Specifically, in Chengdu, photochemical reactions took the lead in
579 escalating O₃ levels (reaching 49.9 ppbv). This could be attributed to a
580 combination of factors. On one hand, being limited to the local air masses,
581 pollutants got accumulated and resulted in the increment of the
582 atmospheric oxidizing capacity. On the other hand, under the influence of
583 conducive meteorological conditions during heatwaves, the vigorous
584 photochemical formation of O₃ was substantially enhanced, resulting in
585 notable O₃ concentration increments. Compared to Chengdu, the
586 contribution of photochemistry to O₃ in Chongqing was nearly half (29.2
587 ppbv). While both photochemical reactions and regional transport



588 positively affected O₃ levels in Chongqing, the overall net accumulation of
589 O₃ was notably lower in this city.



590

591 Fig 10 Averaged contributions of different process to O₃ concentrations at noon time (14:00)
592 in Chengdu and Chongqing

593 4. Conclusion and implication

594 The unprecedented heatwave of August 2022 brought about significant
595 divergence in O₃ levels between Chengdu and Chongqing, with exceeded
596 levels of O₃ appeared in the western SCB (Chengdu) but relatively lower
597 concentrations in the eastern basin (Chongqing). Meteorological and
598 precursor factors were assessed using a machine learning method,
599 spotlighting high temperatures, intensive solar radiation, and overnight
600 accumulative pollutants as key contributors to O₃ concentration. The
601 interplay of isoprene, temperature, and O₃, alongside MEGAN calculations,
602 underscored the intensified BVOCs emissions during heatwaves,
603 highlighting the important role of meteorology-induced natural emissions.
604 Interestingly, BVOCs emissions in Chongqing were nearly twice those in
605 Chengdu; however, their contributions to O₃ concentrations were subdued.
606 This discrepancy was attributed to the distinct responses of O₃-NO_x-VOCs
607 sensitivity mechanisms. Chengdu exhibited sensitivity to VOCs, while



608 Chongqing displayed a transitional sensitivity regime. Considering that
609 China's previous emission reduction strategies have primarily focused on
610 a nationwide NO_x reduction (driven by the need to control PM_{2.5} pollution),
611 it is important to recognize that a short-term reduction in NO_x can lead to
612 an O₃ rebound in regions like Chengdu Plain. To achieve more precise
613 pollution control, a strategy that combines VOCs as the primary focus with
614 concurrent NO_x reductions would be more appropriate. In addition, the
615 investigation into source region contributions revealed varying impacts of
616 regional transport, even within the same basin. Chongqing was
617 significantly influenced by cross-regional transport, whereas Chengdu was
618 predominantly affected by local emissions.

619 These findings illuminate the complex interplay of meteorology, natural
620 emissions, and anthropogenic sources during heatwaves, guiding the
621 necessity of targeted pollution control measures. It is imperative to adopt
622 emission control strategies that are customized according to regional or
623 even local conditions, rather than enforcing uniform measures for the entire
624 region. Given that O₃ pollution is not solely an in-situ problem but rather a
625 regional issue, this concept extends beyond the SCB and is applicable to
626 other urban clusters, such as the Beijing-Tianjin-Hebei region, the Yangtze
627 River Delta region, the Pearl River Delta region, and developed regions in
628 other countries. Future efforts are suggested to focus on regional
629 coordinated and balanced control measures.

630 **Author Contributions**

631 F.Y. and N.W. designed the research. N.W. wrote the manuscript. N.W.,
632 D.Y., C.D., and M.H. contributed to the interpretation of the results. All the
633 authors provided critical feedback and helped to improve the manuscript.

634 **Competing Interests**

635 The authors declare that they have no known competing financial interests
636 or personal relationships that could have appeared to influence the work.

637 **Acknowledgement**

638 This study is supported by the National Natural Science Foundation of
639 China (No. 42175124 and No. 22276128), Science and Technology
640 Department of Sichuan Province (23YFS0383), the Guangdong Basic and
641 Applied Basic Research Foundation (Grant No. 2022A1515011753), the



642 Fundamental Research Funds for the Central Universities (Grant No.
643 YJ202313), and the Young Talent Support Project of Guangzhou
644 Association for Science and Technology (Grant No. QT-2023-048). The
645 authors also thank the Tsinghua University for compiling and sharing the
646 MEIC emission inventory.

647 Reference

- 648 Bloss, C., Wagner, V., Jenkin, M. E., Volkamer, R., Bloss, W. J., Lee, J. D., Heard, D. E., Wirtz, K.,
649 Martin-Reviejo, M., Rea, G., Wenger, J. C., and Pilling, M. J.: Development of a detailed chemical
650 mechanism (MCMv3.1) for the atmospheric oxidation of aromatic hydrocarbons, *Atmos. Chem.*
651 *Phys.*, 5, 641-664, 10.5194/acp-5-641-2005, 2005.
- 652 Cardelino, C. A. and Chameides, W. L.: An Observation-Based Model for Analyzing Ozone
653 Precursor Relationships in the Urban Atmosphere, *Journal of the Air & Waste Management*
654 *Association*, 45, 161-180, 10.1080/10473289.1995.10467356, 1995.
- 655 Chen, D., Zhou, L., Wang, C., Liu, H., Qiu, Y., Shi, G., Song, D., Tan, Q., and Yang, F.: Characteristics
656 of ambient volatile organic compounds during spring O₃ pollution episode in Chengdu, China,
657 *Journal of Environmental Sciences*, 114, 115-125, 2022.
- 658 Daum, P. H., Kleinman, L. I., Springston, S. R., Nunnermacker, L., Lee, Y. N., Weinstein-Lloyd, J.,
659 Zheng, J., and Berkowitz, C. M.: A comparative study of O₃ formation in the Houston urban and
660 industrial plumes during the 2000 Texas Air Quality Study, *Journal of Geophysical Research:*
661 *Atmospheres*, 108, 2003.
- 662 Ding, A., Huang, X., and Fu, C.: Air pollution and weather interaction in East Asia, in: *Oxford*
663 *Research Encyclopedia of Environmental Science*, 2017.
- 664 Emberson, L., Ashmore, M., Murray, F., Kuylensstierna, J., Percy, K., Izuta, T., Zheng, Y., Shimizu, H.,
665 Sheu, B., and Liu, C.: Impacts of air pollutants on vegetation in developing countries, *Water, Air,*
666 *and Soil Pollution*, 130, 107-118, 2001.
- 667 Hall, S. J., Matson, P. A., and Roth, P. M.: NO_x emissions from soil: implications for air quality
668 modeling in agricultural regions, *Annual Review of Energy and the Environment*, 21, 311-346, 1996.
- 669 Hu, J., Zhao, T., Liu, J., Cao, L., Wang, C., Li, Y., Shi, C., Tan, C., Sun, X., and Shu, Z.: Exploring the
670 ozone pollution over the western Sichuan Basin, Southwest China: The impact of diurnal change
671 in mountain-plains solenoid, *Science of The Total Environment*, 839, 156264, 2022.
- 672 Huang, J., Hartmann, H., Hellén, H., Wisthaler, A., Perreca, E., Weinhold, A., Ruckner, A., van Dam,
673 N. M., Gershenzon, J., and Trumbore, S.: New perspectives on CO₂, temperature, and light effects
674 on BVOC emissions using online measurements by PTR-MS and cavity ring-down spectroscopy,
675 *Environmental science & technology*, 52, 13811-13823, 2018.
- 676 Jacob, D. J.: Heterogeneous chemistry and tropospheric ozone, *Atmospheric Environment*, 34,
677 2131-2159, 2000.
- 678 Jenkin, M. E. and Clemitshaw, K. C.: Ozone and other secondary photochemical pollutants:
679 chemical processes governing their formation in the planetary boundary layer, *Atmospheric*
680 *Environment*, 34, 2499-2527, 2000.
- 681 Jenkin, M. E., Saunders, S. M., and Pilling, M. J.: The tropospheric degradation of volatile organic
682 compounds: a protocol for mechanism development, *Atmospheric Environment*, 31, 81-104,
683 [https://doi.org/10.1016/S1352-2310\(96\)00105-7](https://doi.org/10.1016/S1352-2310(96)00105-7), 1997.



- 684 Jenkin, M. E., Young, J. C., and Rickard, A. R.: The MCM v3.3.1 degradation scheme for isoprene,
685 *Atmos. Chem. Phys.*, 15, 11433-11459, 10.5194/acp-15-11433-2015, 2015.
- 686 Jenkin, M. E., Saunders, S. M., Wagner, V., and Pilling, M. J.: Protocol for the development of the
687 Master Chemical Mechanism, MCM v3 (Part B): tropospheric degradation of aromatic volatile
688 organic compounds, *Atmos. Chem. Phys.*, 3, 181-193, 10.5194/acp-3-181-2003, 2003.
- 689 Krupa, S. V. and Kickert, R. N.: The greenhouse effect: impacts of ultraviolet-B (UV-B) radiation,
690 carbon dioxide (CO₂), and ozone (O₃) on vegetation, *Environmental Pollution*, 61, 263-393, 1989.
- 691 Kwok, R. H., Napelenok, S. L., and Baker, K. R.: Implementation and evaluation of PM_{2.5} source
692 contribution analysis in a photochemical model, *Atmospheric Environment*, 80, 398-407, 2013.
- 693 Lei, Y., Wu, K., Zhang, X., Kang, P., Du, Y., Yang, F., Fan, J., and Hou, J.: Role of meteorology-driven
694 regional transport on O₃ pollution over the Chengdu Plain, southwestern China, *Atmospheric
695 Research*, 285, 106619, 2023.
- 696 Lelieveld, J. and Dentener, F. J.: What controls tropospheric ozone?, *Journal of Geophysical
697 Research: Atmospheres*, 105, 3531-3551, 10.1029/1999jd901011, 2000.
- 698 Lu, X., Zhang, L., and Shen, L.: Meteorology and Climate Influences on Tropospheric Ozone: a
699 Review of Natural Sources, Chemistry, and Transport Patterns, *Current Pollution Reports*, 5, 238-
700 260, 10.1007/s40726-019-00118-3, 2019.
- 701 McElroy, M. B., Salawitch, R. J., and Wofsy, S. C.: Antarctic O₃: Chemical mechanisms for the spring
702 decrease, *Geophysical research letters*, 13, 1296-1299, 1986.
- 703 Meng, X., Jiang, J., Chen, T., Zhang, Z., Lu, B., Liu, C., Xue, L., Chen, J., Herrmann, H., and Li, X.:
704 Chemical drivers of ozone change in extreme temperatures in eastern China, *Science of The Total
705 Environment*, 874, 162424, <https://doi.org/10.1016/j.scitotenv.2023.162424>, 2023.
- 706 Napelenok, S., Cohan, D., Odman, M. T., and Tonse, S.: Extension and evaluation of sensitivity
707 analysis capabilities in a photochemical model, *Environmental Modelling & Software*, 23, 994-999,
708 2008.
- 709 Potosnak, M. J., LeStourgeon, L., Pallardy, S. G., Hosman, K. P., Gu, L., Karl, T., Geron, C., and
710 Guenther, A. B.: Observed and modeled ecosystem isoprene fluxes from an oak-dominated
711 temperate forest and the influence of drought stress, *Atmospheric Environment*, 84, 314-322, 2014.
- 712 Qiao, X., Guo, H., Wang, P., Tang, Y., Ying, Q., Zhao, X., Deng, W., and Zhang, H.: Fine particulate
713 matter and ozone pollution in the 18 cities of the Sichuan Basin in southwestern China: model
714 performance and characteristics, *Aerosol and Air Quality Research*, 19, 2308-2319, 2019.
- 715 Saunders, S. M., Jenkin, M. E., Derwent, R. G., and Pilling, M. J.: Protocol for the development of
716 the Master Chemical Mechanism, MCM v3 (Part A): tropospheric degradation of non-aromatic
717 volatile organic compounds, *Atmos. Chem. Phys.*, 3, 161-180, 10.5194/acp-3-161-2003, 2003.
- 718 Saunier, A., Ormeño, E., Boissard, C., Wortham, H., Temime-Roussel, B., Lecareux, C., Armengaud,
719 A., and Fernandez, C.: Effect of mid-term drought on *Quercus pubescens* BVOCs' emission
720 seasonality and their dependency on light and/or temperature, *Atmospheric Chemistry and
721 Physics*, 17, 7555-7566, 2017.
- 722 Schwela, D.: Air pollution and health in urban areas, *Reviews on environmental health*, 15, 13-42,
723 2000.
- 724 Shu, Z., Zhao, T., Liu, Y., Zhang, L., Ma, X., Kuang, X., Li, Y., Huo, Z., Ding, Q., and Sun, X.: Impact of
725 deep basin terrain on PM_{2.5} distribution and its seasonality over the Sichuan Basin, Southwest
726 China, *Environmental Pollution*, 300, 118944, 2022.
- 727 Wang, H., Lu, X., Seco, R., Stavrou, T., Karl, T., Jiang, X., Gu, L., and Guenther, A. B.: Modeling



728 Isoprene Emission Response to Drought and Heatwaves Within MEGAN Using Evapotranspiration
729 Data and by Coupling With the Community Land Model, *Journal of advances in modeling earth*
730 *systems*, 14, e2022MS003174, 10.1029/2022MS003174, 2022a.

731 Wang, N., Guo, H., Jiang, F., Ling, Z., and Wang, T.: Simulation of ozone formation at different
732 elevations in mountainous area of Hong Kong using WRF-CMAQ model, *Science of the total*
733 *environment*, 505, 939–951, 2015.

734 Wang, N., Huang, X., Xu, J., Wang, T., Tan, Z.-m., and Ding, A.: Typhoon-boosted biogenic emission
735 aggravates cross-regional ozone pollution in China, *Science Advances*, 8, eabl6166, 2022b.

736 Wang, P., Qiao, X., and Zhang, H.: Modeling PM_{2.5} and O₃ with aerosol feedbacks using
737 WRF/Chem over the Sichuan Basin, southwestern China, *Chemosphere*, 254, 126735, 2020.

738 Wang, T., Xue, L., Brimblecombe, P., Lam, Y. F., Li, L., and Zhang, L.: Ozone pollution in China: A
739 review of concentrations, meteorological influences, chemical precursors, and effects, *Science of*
740 *the Total Environment*, 575, 1582–1596, 2017.

741 Xiao, Q., Geng, G., Xue, T., Liu, S., Cai, C., He, K., and Zhang, Q.: Tracking PM_{2.5} and O₃ pollution
742 and the related health burden in China 2013–2020, *Environmental science & technology*, 56, 6922–
743 6932, 2021.

744 Xue, L., Wang, T., Wang, X., Blake, D. R., Gao, J., Nie, W., Gao, R., Gao, X., Xu, Z., Ding, A., Huang,
745 Y., Lee, S., Chen, Y., Wang, S., Chai, F., Zhang, Q., and Wang, W.: On the use of an explicit chemical
746 mechanism to dissect peroxy acetyl nitrate formation, *Environ Pollut*, 195, 39–47,
747 10.1016/j.envpol.2014.08.005, 2014.

748 Zhang, Y., Sun, J., Zheng, P., Chen, T., Liu, Y., Han, G., Simpson, I. J., Wang, X., Blake, D. R., Li, Z.,
749 Yang, X., Qi, Y., Wang, Q., Wang, W., and Xue, L.: Observations of C-1-C-5 alkyl nitrates in the
750 Yellow River Delta, northern China: Effects of biomass burning and oil field emissions, *Science of*
751 *the Total Environment*, 656, 129–139, 10.1016/j.scitotenv.2018.11.208, 2019.

752 Zhao, S., Yu, Y., Yin, D., Qin, D., He, J., and Dong, L.: Spatial patterns and temporal variations of six
753 criteria air pollutants during 2015 to 2017 in the city clusters of Sichuan Basin, China, *Science of*
754 *the Total Environment*, 624, 540–557, 2018.

755 Zhou, Z., Tan, Q., Deng, Y., Song, D., Wu, K., Zhou, X., Huang, F., Zeng, W., and Lu, C.: Compilation
756 of emission inventory and source profile database for volatile organic compounds: A case study
757 for Sichuan, China, *Atmospheric Pollution Research*, 11, 105–116, 2020.

758 Zhu, J. X., Cheng, H. R., Peng, J., Zeng, P., Wang, Z. W., Lyu, X. P., and Guo, H.: O-3 photochemistry
759 on O-3 episode days and non-O-3 episode days in Wuhan, Central China, *Atmospheric*
760 *Environment*, 223, 10.1016/j.atmosenv.2019.117236, 2020.

761